

Tunable colossal negative magnetoresistance of topological semimetal EuB_6 thin sheets

Ke Zhu(祝轲), Qi Qi(齐琦), Yaofeng Xie(谢耀锋), Lulu Pan(潘禄禄), Senhao Lv(吕森浩), Guojing Hu(胡国静), Zhen Zhao(赵振), Guoyu Xian(冼国裕), Yechao Han(韩烨超), Lihong Bao(鲍丽宏), Ying Zhang(张颖), Xiao Lin(林晓), Hui Guo(郭辉), Haitao Yang(杨海涛), and Hong-Jun Gao(高鸿钧)

Citatio: Chin. Phys. B, 2025, 34 (**9**): 097308. DOI: 10.1088/1674-1056/add5ca
http://cpb.iphy.ac.cn; http://iopscience.iop.org/cpb

What follows is a list of articles you may be interested in

Observation of distinct Kondo effect and anomalous Hall effect in V self-intercalated layered antiferromagnet V_5S_8 crystals

Yaofeng Xie(谢耀锋), Senhao Lv(吕森浩), Qi Qi(齐琦), Guojing Hu(胡国静), Ke Zhu(祝轲), Zhen Zhao(赵振), Guoyu Xian(冼国裕), Yechao Han(韩烨超), Ruwen Wang(王汝文), Chenyu Bai(白晨宇), Lihong Bao(鲍丽宏), Xiao Lin(林晓), Hui Guo(郭辉), Haitao Yang(杨海涛), and Hong-Jun Gao(高鸿钧)

Chin. Phys. B, 2025, 34 (**8**): 087303. DOI: 10.1088/1674-1056/add5cd

In-plane negative magnetoresistance and quantum oscillations in van der Waals antiferromagnet $DyTe_3$

Qi Qi(齐琦), Senhao Lv(吕森浩), Ke Zhu(祝轲), Yaofeng Xie(谢耀锋), Guojing Hu(胡国静), Zhen Zhao(赵振), Guoyu Xian(冼国裕), Yechao Han(韩烨超), Yang Yang(杨洋), Lihong Bao(鲍丽宏), Xiao Lin(林晓), Hui Guo(郭辉), Haitao Yang(杨海涛), and Hong-Jun Gao(高鸿钧)

Chin. Phys. B, 2025, 34 (**7**): 077305. DOI: 10.1088/1674-1056/adcc87

Nonlinear current response and electric quantum oscillations in the Dirac semimetal Cd_3As_2

Hao-Nan Cui(崔浩楠), Ze-Nan Wu(吴泽南), Jian-Kun Wang(王建坤), Guang-Yu Zhu(祝光宇), Jia-Jie Yang(杨佳洁), Wen-Zhuang Zheng(郑文壮), Zhi-Min Liao(廖志敏), Shuo Wang(王硕), Ben-Chuan Lin(林本川), and Dapeng Yu(俞大鹏)

Chin. Phys. B, 2023, 32 (**8**): 087306. DOI: 10.1088/1674-1056/acd9c5

Electrical spin polarization through spin-momentum locking in topological-insulator nanostructures

Minhao Zhang(张敏昊), Xuefeng Wang(王学锋), Fengqi Song(宋凤麒), Rong Zhang(张荣)

Chin. Phys. B, 2018, 27 (**9**): 097307. DOI: 10.1088/1674-1056/27/9/097307

Electronic transport properties of Co cluster-decorated graphene

Chao-Yi Cai(蔡超逸), Jian-Hao Chen(陈剑豪)

Chin. Phys. B, 2018, 27 (**6**): 067304. DOI: 10.1088/1674-1056/27/6/067304

Tunable colossal negative magnetoresistance of topological semimetal EuB_6 thin sheets

Ke Zhu(祝轲)[1,2,†], Qi Qi(齐琦)[1,2,†], Yaofeng Xie(谢耀锋)[1,2], Lulu Pan(潘禄禄)[1], Senhao Lv(吕森浩)[1], Guojing Hu(胡国静)[1], Zhen Zhao(赵振)[1], Guoyu Xian(冼国裕)[3], Yechao Han(韩烨超)[2], Lihong Bao(鲍丽宏)[1,2,3], Ying Zhang(张颖)[1,2], Xiao Lin(林晓)[2], Hui Guo(郭辉)[1,2], Haitao Yang(杨海涛)[1,2,‡], and Hong-Jun Gao(高鸿钧)[1,2,§]

[1] *Beijing National Center for Condensed Matter Physics and Institute of Physics, Chinese Academy of Sciences, Beijing* 100190, *China*
[2] *School of Physical Sciences, University of Chinese Academy of Sciences, Beijing* 100049, *China*
[3] *Songshan Lake Materials Laboratory, Dongguan* 523808, *China*

(Received 7 March 2025; revised manuscript received 22 April 2025; accepted manuscript online 8 May 2025)

EuB_6, a magnetic topological semimetal, has attracted considerable attention in recent years due to its rich intriguing physical properties, including a colossal negative magnetoresistance (CNMR) ratio exceeding −80%, a topological phase transition and a predicted quantum anomalous Hall effect (QAHE) approaching the two-dimensional (2D) limit. Yet, studies of the influence of the dimensionality approaching 2D on the electronic transport properties of EuB_6 are still scarce. In this work, EuB_6 thin sheets with thicknesses ranging from 35 μm to 180 μm were successfully fabricated through careful mechanical polishing of high-quality EuB_6 single crystals. The reduced thickness, temperature and magnetic field have a strong influence on the electronic transport properties, including the CNMR and carrier concentration of EuB_6 thin sheets. As the thickness of EuB_6 thin sheets decreases from 180 μm to 35 μm, the magnetization transition temperature and the corresponding suppressing temperature of the Kondo effect decrease from 15.2 K to 10.9 K, while the CNMR ratio increases from −87.2% to −90.8%. Furthermore, the weak antilocalization effect transits to a weak localization effect and the carrier concentration increases by 9.4% at 30 K in a 35 μm EuB_6 thin sheet compared to the value reported for a 180 μm thin sheet. Our findings demonstrate an obvious tunable effect of the reduced dimensionality on the transport properties of EuB_6 along with the temperature and magnetic field, which could provide a route to exploring the QAHE near the 2D limit in EuB_6 and other topological semimetals.

Keywords: EuB_6 thin sheets, magnetic topological semimetal, negative magnetoresistance, Kondo effect, weak localization

PACS: 73.23.–b

DOI: 10.1088/1674-1056/add5ca **CSTR:** 32038.14.CPB.add5ca

1. Introduction

Magnetic topological materials are of particular interest due to the interaction between intrinsic magnetism and topology, and they hold great potential for the development of chiral Majorana edge modes, resistance standards and dissipationless electronic devices.[1–4] Based on topological insulators (TIs) with a magnetic dopant and intrinsic magnetism, the quantum anomalous Hall effect (QAHE) has been realized in Cr- or V-doped $(Bi,Sb)_2Te_3$ films[5–15] and exfoliated $MnBi_2Te_4$ flakes.[16] Besides TIs, topological semimetals emerged as novel states of matter where the valence and conduction bands touch at either discrete points or extended lines, forming Dirac/Weyl semimetals and nodal line semimetals.[17,18] Many materials have been predicted and demonstrated to be topological semimetals, most of which are time-reversal invariant. Only a few materials have been studied as magnetic topological semimetals, such as $Co_3Sn_2S_2$,[19] Fe_3Sn_2[20] and $GdAg_2$.[21] In the two-dimensional (2D) limit, these systems with gapped Dirac cones can be viewed as Chern insulators with quantized anomalous Hall conductance.[22,23] In this sense, these materials share the same topological characters (the Chern number) as intrinsic magnetic TIs.

EuB_6 possesses a simple cubic crystal structure and is a magnetic topological nodal-line semimetal at low temperatures. It is a soft ferromagnetic semimetal with very low magnetic anisotropy energy, so its magnetization can be easily modulated by a magnetic field. By breaking certain crystalline symmetry, EuB_6 can be driven into Weyl semimetals[24] or a composite phase with coexisting nodal line and Weyl points.[25] Magnetic Weyl semimetals can be viewed as a stack of two-dimensional Chern insulators with strong coupling in the stacking direction. Moreover, according to theoretical calculations, EuB_6 is predicted to realize a large-Chern-number QAHE in its [111]-oriented quantum-well structures.[25] Thus, EuB_6 is an ideal platform upon which to reveal exotic transport properties and the correlation between magnetism and topology. In experimental studies of EuB_6, colossal negative magnetoresistance (CNMR),[26,27] as well as topological tran-

†These authors contributed equally to this work.
‡Corresponding author. E-mail: htyang@iphy.ac.cn
§Corresponding author. E-mail: hjgao@iphy.ac.cn

© 2025 Chinese Physical Society and IOP Publishing Ltd. All rights, including for text and data mining, AI training, and similar technologies, are reserved.

sitions induced by the spontaneous ferromagnetism and magnetic field, have been reported.[28] Nonetheless, reports of the electronic transport properties of EuB_6 thin sheets toward the 2D limit are still scarce.

In this paper, a high-quality EuB_6 single crystal is prepared by an Al-flux method.[29] EuB_6 thin sheets, with thicknesses ranging from 35 μm to 180 μm, are carefully then fabricated by mechanical polishing of the EuB_6 single crystal. The resistivity (ρ_{xx}), magnetoresistance (MR) and Hall resistivity (ρ_{xy}) of the EuB_6 thin sheets with different thicknesses are measured, revealing the strong influence of the reduced dimension, temperature and magnetic field on the transport properties. As the thickness of EuB_6 thin sheets decreases from 180 μm to 35 μm, the magnetization transition temperature and the corresponding suppressing temperature of the Kondo effect decrease from 15.2 K to 10.9 K, while the CNMR ratio increases from −87.2% to −90.8%. Furthermore, the weak antilocalization (WAL) effect transits to a weak localization (WL) effect and the carrier concentration shows an increase of 9.4% at 30 K in the 35 μm EuB_6 thin sheet compared to the value of the 180 μm thin sheet. Our findings demonstrate an obvious modulation effect of the reduced dimensionality on the transport properties of EuB_6 along with its temperature and magnetic field. The results are applicable to other topological systems with strong correlations between conducting electrons and local magnetic moments, and furthermore provides a route to manipulating the topology-related transport properties in magnetic topological materials through the reduced dimension.

2. Experiment

Single crystals of EuB_6 were grown by an Al-flux method.[29] The Eu (99.99%) pieces and B (99%) powder mixture were placed in an alumina crucible and heated in a horizontal tube furnace with an argon flow of 100 SCCM maintained throughout the whole growth process. The mixture was heated to 1500 °C and held at that temperature for 72 h, subsequently cooled to 1200 °C at 2 °C/ h and then to 900 °C at 2.5 °C/ h. The furnace was shut down and then cooled to room temperature naturally. The crystals were finally separated by dissolving the excess Al-flux in hydrochloric acid solution. The obtained crystals had a typical quadrate morphology, were millimeter-sized and stable in air.

The EuB_6 thin sheets with thicknesses ranging from 35 μm to 180 μm were fabricated by using a careful mechanical polishing technique. Firstly, a rectangular EuB_6 single crystal with ∼ mm thickness was stuck onto a glass slide and fixed onto the sample holder, then it was reduced to the desired thickness by slow polishing on the waterproof abrasive papers in an Allied Multiprep-10-1110 polishing machine. Finally, the electrodes were fabricated on EuB_6 thin sheets using wire-bonding equipment.

3. Results and discussion

EuB_6 has a simple cubic crystal structure, with Eu atoms constituting a simple cubic lattice and a regular boron octahedron positioned at the body center. Figure 1(a) shows the three-dimensional diagram and the front view (observed along a axis) of the EuB_6 crystal lattice with the Pm-3m(221) space group and the lattice constant $a = b = c = 4.185$ Å. The as-grown EuB_6 single crystal has a perfect rectangle shape with sharply natural edges (Fig. 1(b)), corresponding to the cubic crystal symmetry of EuB_6. The length of a single crystal is about 1–3 mm. The XRD pattern (as shown in Fig. S1(a)), measured with the natural surface of the crystal stacking to the sample holder plane, shows only the {001} crystal plane family of EuB_6. The corresponding XRD pattern of EuB_6 powders, obtained by grinding the as-grown EuB_6 single crystal, is shown in Fig. S1(b), where both the peak positions and intensities perfectly match the standard pattern (PDF-#65-5933). The high-resolution transmission electron microscopy (HRTEM) image measured along the [001] direction shows a lattice constant of 4.19 Å along the a or b axis (Fig. 1(c)), which is consistent with that acquired from the XRD measurement. The selected area electron diffraction (SAED) image (Fig. S1(c)) clearly shows the cubic crystal symmetry of the EuB_6 single crystal. The diffraction spots of the (010) and (110) crystal planes are marked by yellow circles in the image. By fitting the energy dispersive x-ray (EDX) spectrum (Fig. S1(d)), the atomic ratio of Eu and B is demonstrated to be Eu:B = 1:6.06, close to the stoichiometric ratio of EuB_6.

To explore the influence of the reduced dimension on the transport properties of EuB_6, EuB_6 thin sheets with different thicknesses of 180 μm, 90 μm, 62 μm and 35 μm are investigated in this work. The SEM image of the cross-section shows that the thin sheet fabricated by fine polishing possesses a flat surface and uniform thickness of 35 μm (Fig. 1(e)). Figure 1(f) is the Raman spectra of different EuB_6 thin sheets. The spectra of the 180 μm and 35 μm thin sheets are almost coincident, showing typical T_{2g}, E_g, and A_{1g} peaks of EuB_6[30] at 768 cm^{-1}, 1098 cm^{-1}, and 1239 cm^{-1}. The narrow Raman peaks indicate the high quality and good homogeneity of the EuB_6 thin sheets.

The magnetic properties of EuB_6 thin sheets with different thicknesses were first measured to determine the ferromagnetic–paramagnetic (FM–PM) transition temperature and magnetization strength. The temperature-dependent magnetization (M–T) measurements in the zero-field-cooling (ZFC) and field-cooling (FC) procedures show different FM–PM transition temperatures for 180 μm and 35 μm EuB_6 thin sheets. For the 180 μm thin sheet, the magnetization measured under 0.005 T remains approximately constant from 2 K to 8 K (Fig. 2(a)), indicating a fully FM state along the [111] direction.[31] Between 8 K and 20 K, the corresponding dM/dT–T curve shows two downward peaks (shown in the

inset of Fig. 2(a)), which indicates that the EuB_6 thin sheet undergoes two magnetic phase transitions at 11.4 K and 14.8 K. This result reveals that the spin orientation along the [111] direction and along the [100] direction remain in the 180 μm EuB_6 thin sheet, which is consistent with the reported results for EuB_6 single crystals.[31] Then a gentle continuous decrement from 20 K to 50 K indicates the transition to a PM state (Figs. 2(a) and 2(b)). While, for the 35 μm thin sheet, the FM–PM phase transition still exists, but only one obvious downward peak at 10.7 K can be observed in the dM/dT–T curve (shown in the inset of Fig. 2(b)), which indicates that the spin orientation along the [100] transition near 14.8 K is strongly suppressed by the decreased thickness. Meanwhile, the magnetic field-dependent magnetization (M–B) curves of EuB_6 thin sheets with thicknesses of 180 μm and 35 μm were measured at different temperatures (shown in Figs. S2(a) and S2(b)). The M–B curves show no hysteresis even under a field of 7 T at 2 K. The saturation magnetization (M_s) values of the 180 μm and 35 μm thin sheets are about 1.21 T and 1.24 T at 2 K, corresponding to about 7.61 μ_B and 7.8 μ_B per unit cell, which indicates a slight increment of M_s. M_s gradually decreases with an increase of temperature from 20 K to 30 K until an obvious PM behavior appears above 30 K.

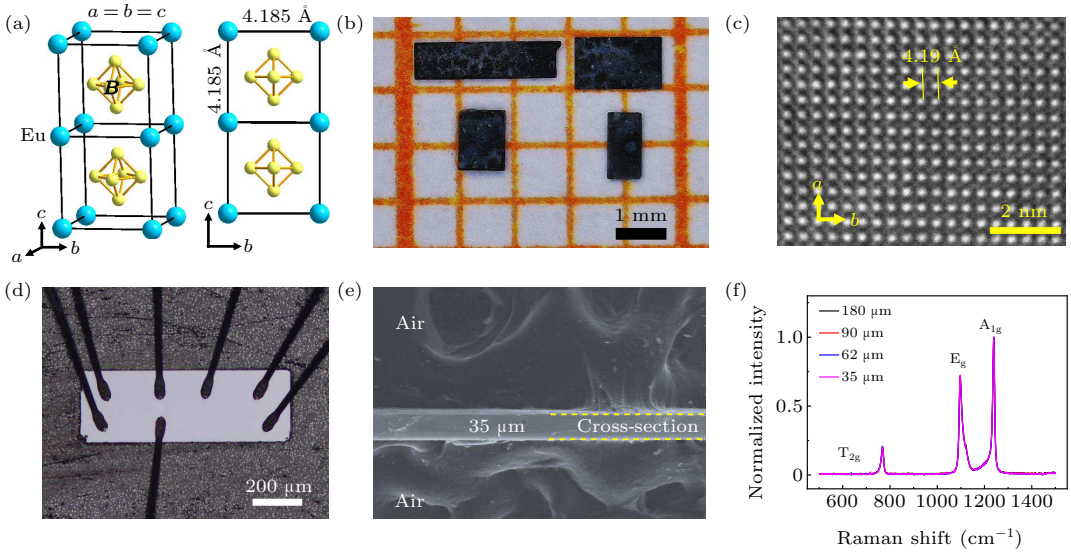


Fig. 1. (a) The diagram of the EuB_6 lattice structure. Eu atoms constitute a simple cubic lattice with a regular octahedron located at the body center. (b) The optical photograph of typical as-grown EuB_6 single crystals with a square shape. (c) HRTEM image measured along the [001] direction of the EuB_6 single crystal, showing a high-quality crystalline lattice. (d) The optical macroscope image of the EuB_6 thin sheets device fabricated by mechanical polishing. (e) The SEM image of the corresponding cross-section of the thin sheet, which shows the thickness to be about 35 μm. (f) Raman spectra of EuB_6 single crystals with different thicknesses.

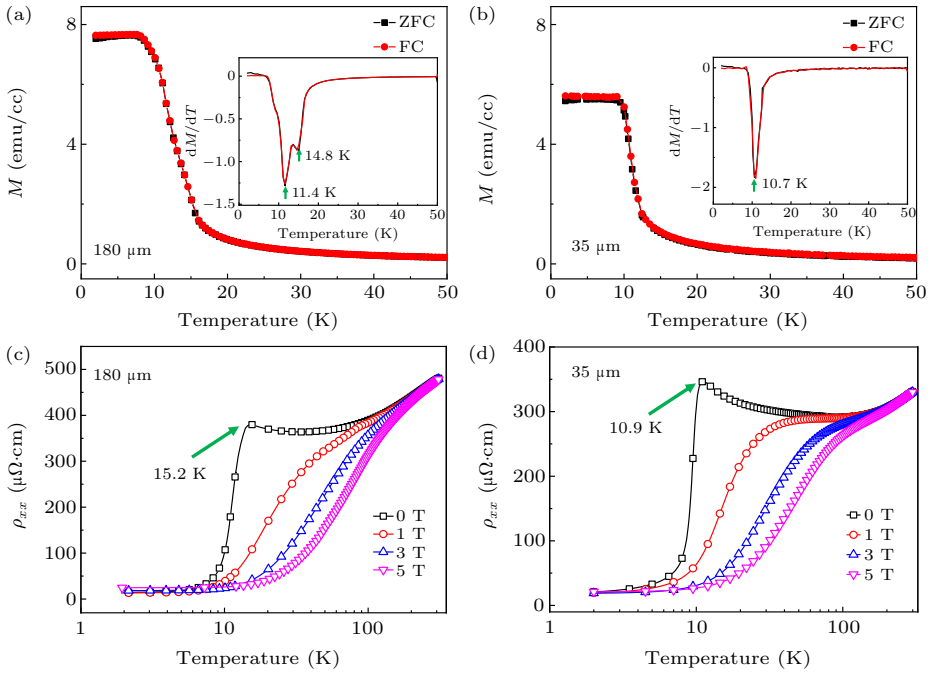


Fig. 2. (a) and (b) The M–T curves of EuB_6 thin sheets with thicknesses of 180 μm and 35 μm. The inset is the temperature-dependent dM/dT–T curve derived from the M–T curve measured under 0.005 T. (c) and (d) ρ_{xx}–T curves of EuB_6 thin sheets with thicknesses of 180 μm and 35 μm.

The ρ_{xx}–T curves of different EuB_6 thin sheets were measured based on the electrode configuration shown in Fig. 1(d). For the 180 μm EuB_6 thin sheet, in the absence of the external magnetic field, ρ_{xx} first decreases as the temperature decreases from 300 K to 50 K due to the weakening of the scattering effect between electrons and phonons (shown in Fig. 2(c)). Then ρ_{xx} increases from a minimum value of 363.9 μΩ·cm to a local maximum value of 379.6 μΩ·cm as the temperature decreases from 50 K to 15.2 K due to the Kondo effect arising from the generation of ferromagnetic clusters. Subsequently, the ρ_{xx} dramatically decreases below 15 K owing to the spontaneous ferromagnetism-induced topological transition in EuB_6.[24,32] While, under applied magnetic fields, the Kondo-like upwarp of ρ_{xx} is suppressed and ρ_{xx} decreases monotonically from 300 K to 1.9 K. The decrease of ρ_{xx} is mainly from the inherent spontaneous ferromagnetism induced topological transition in EuB_6, which can reduce electron scattering. Below 8 K, ρ_{xx} tends to be a constant because the spontaneous magnetization reaches saturation. For the 35 μm EuB_6 thin sheets, the ρ_{xx}–T curves show a similar behavior except for a local maximum value at ∼ 10.9 K corresponding to the FM–PM transition temperature, which indicates that the Kondo effect in EuB_6 thin sheets is mainly determined by local moments.

The MR curves of EuB_6 thin sheets were measured at different temperatures, as shown in Fig. 3. The MR ratio is defined as $[\rho_{xx}(B) - \rho_{xx}(0)]/\rho_{xx}(0)$, where $\rho_{xx}(0)$ and $\rho_{xx}(B)$ are the longitudinal resistivities under the zero and finite external magnetic fields, respectively (the original measurement data in Fig. S3). Overall, the MR curves decrease firstly and then increase with the external magnetic field increasing. The external magnetic field corresponding to the maximum negative MR ratio is defined as the critical magnetic field (B_c@MR, where the δMR = 0). To reveal the influence of thickness on MR, the thickness-dependent MR curves at 1.9 K and B_c@MR at different temperatures are depicted in Figs. 3(c) and 3(d). For the 180 μm EuB_6 thin sheet, the MR curves ranging from −1.5 T to +1.5 T do not show the distinctive sharp cusps corresponding to the WL effect,[33] but rather a slight increment near the zero field that might have arisen from the WAL effect. From 10 K to 35 K, it can be found that the temperature and external critical magnetic field both have an influence on the maximum negative MR ratio and a CNMR ratio exceeding −87.2% is achieved around 12 K. According to our previous research results,[27] the WL effect cannot be the dominated mechanism for CNMR. In addition, the negative MR ratio contributed by the Kondo upwarp is only about $(363.9 - 379.6)/379.6 \approx -4.1\%$ in the 180 μm EuB_6 thin sheet, which is much less than the CNMR ratio ∼ −87.2%. When the thickness decreases below 90 μm, a WL effect can be observed between −1 T to 1 T. Meanwhile, below 20 K, B_c@MR shows an obvious increase when the thickness decreases below 90 μm. It should be noted that though the existence of WL in EuB_6 thin sheets with a thickness below 90 μm, the magnetic field-induced topological phase transition is still the main mechanism for CNMR since all CNMR ratios for EuB_6 thin sheets below 90 μm are over −89.5% and, especially, the CNMR ratio for 35 μm EuB_6 thin sheet reaches −90.8% (Fig. S4(d)).[27]

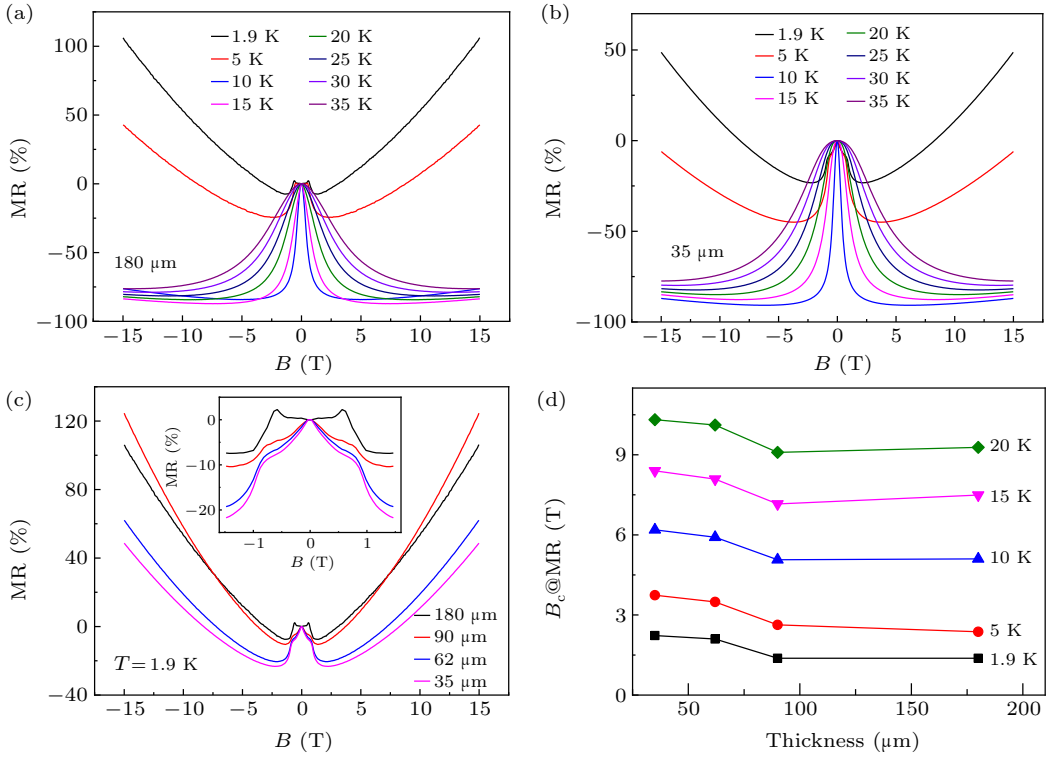


Fig. 3. (a) and (b) MR ratio curves of EuB_6 thin sheets with thicknesses of 180 μm and 35 μm. (c) Corresponding MR ratio curves of EuB_6 thin sheets with different thicknesses measured at 1.9 K. (d) Thickness-dependent B_c@MR of different EuB_6 thin sheets at different temperatures.

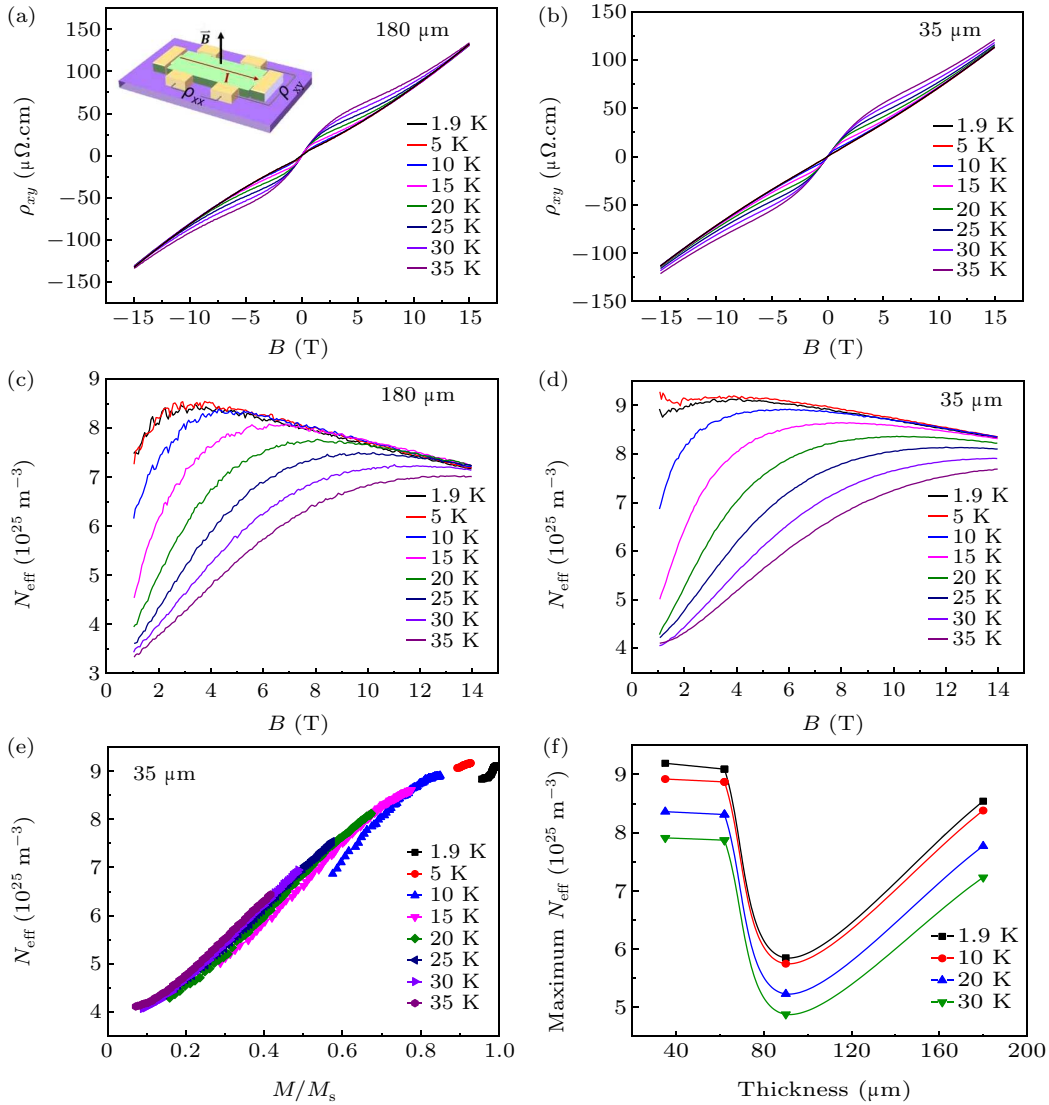


Fig. 4. (a) and (c) Hall resistivity of EuB_6 thin sheets. (b) and (d) Field-dependent effective carrier concentration ($N_{\rm eff}$) of EuB_6 thin sheets with thicknesses of 180 μm and 35 μm. (e) Effective carrier concentration dependency of the field induced magnetization ratio. (f) Thickness-dependent maximum effective carrier concentration at different temperatures.

Such huge CNMR ratios mean an approximate eightfold reduction of ρ_{xx} as the external magnetic field increases from zero to $B_{\rm c}$, which is impossible to explain only by the suppression of the scattering between carriers and the magnetic moments under the applied magnetic field.[34] Fundamentally, the carrier concentration mainly determines the electronic resistivity. Hence, variations in the carrier concentration of EuB_6 thin sheets are further investigated through Hall resistivity measurements, which can well reflect the carrier concentration in EuB_6 thin sheets. The field-dependent ρ_{xy} of EuB_6 thin sheets with thicknesses of 180 μm and 35 μm is measured at different temperatures (shown in Figs. 4(a) and 4(b)). Similar to the EuB_6 bulk, ρ_{xy} without the linear dependence of the external magnetic field is observed from 1.9 K to 35 K in EuB_6 thin sheets. The nonlinear dependence behavior becomes more distinct as the temperature increases. For further clarification, the $N_{\rm eff}$ curves of EuB_6 thin sheets with thicknesses of 180 μm and 35 μm have been derived from ρ_{xy} (shown in Figs. 4(c) and 4(d)). $N_{\rm eff}$ initially increases and then slightly decreases with the external magnetic field increasing. In contrast, $N_{\rm eff}$ always increases with a decrease in temperature. Moreover, the field-induced magnetization ratio ($M/M_{\rm s}$) dependence of $N_{\rm eff}$ (Fig. 4(e)) indicates that the carrier pocket as well as the electron band structures near the Fermi level can be effectively changed by the magnetic field-induced magnetization. This phenomenon is analogous to the reported temperature-induced variation of the band structures in EuB_6 bulk.[24,32] In addition, we find that $N_{\rm eff}$ reaches its maximum value under the critical magnetic field ($B_{\rm c}@N_{\rm eff}$) where $\delta N_{\rm eff} = 0$ at different temperatures from 1.9 K to 35 K. Interestingly, the maximum $N_{\rm eff}$ corresponds to the maximum CNMR ratio, which indicates the field-induced variation of $N_{\rm eff}$ should be responsible for CNMR in EuB_6 thin sheets. The maximum $N_{\rm eff}$ for EuB_6 thin sheets with different thicknesses at various temperatures is depicted in Fig. 4(f). Overall, the maximum $N_{\rm eff}$ increases as the thickness decreases. To

be more specific, the maximum $N_{\rm eff}$ decreases with the thickness decreasing from 180 μm to 90 μm, then increases from 90 μm to 35 μm (Figs. S5 and S6). The maximum $N_{\rm eff}$ of the 35 μm EuB_6 thin sheet shows a 9.4% increment compared to that of the sample with 180 μm at 30 K. The maximum carrier mobility values of EuB_6 thin sheets with thicknesses of 35 μm, 62 μm, 90 μm and 180 μm are 2943 $cm^2 \cdot V^{-1} \cdot s^{-1}$, 2817 $cm^2 \cdot V^{-1} \cdot s^{-1}$, 3894 $cm^2 \cdot V^{-1} \cdot s^{-1}$ and 3192 $cm^2 \cdot V^{-1} \cdot s^{-1}$ at 1.9 K (Fig. S7), respectively. A comparison of the performance parameters between the bulk and thin-sheet forms of EuB_6 is presented in Fig. S8. Thus, the thickness-dependent maximum $N_{\rm eff}$, modulated by the magnetization states, begins to exhibit a noticeable variation around 90 μm, likely due to changes in the demagnetizing field and magnetization dynamics as the sample thickness decreases, indicating the onset of discernible thickness-dependent behavior.

4. Conclusion

In conclusion, we have successfully fabricated EuB_6 thin sheets with thicknesses ranging from 35 μm to 180 μm through careful mechanical polishing of high-quality EuB_6 single crystals. The reduced dimension, temperature and magnetic field have a strong influence on the electronic transport properties, including CNMR and carrier concentration, of the EuB_6 thin sheets. The FM–PM phase transition temperature and the corresponding suppressing temperature of Kondo effect decrease from 15.2 K to 10.9 K as the thickness of EuB_6 thin sheets decreases from 180 μm to 35 μm. Below 90 μm, the WAL[35,36] effect transits to the WL effect and the maximum carrier concentration increases by 9.4% compared to the value of the 180 μm thin sheet. Based on the MR and Hall resistivity results, we found a significant modulation of the transport properties upon reducing the material thickness below 90 μm. Our findings demonstrate an obvious modulation effect of the reduced thickness on the transport properties of EuB_6 as well as temperatures and magnetic fields, which could provide a route to explore QAHEs in the two-dimensional limit in EuB_6 and other topological semimetals.

Acknowledgments

Project supported by the National Key R&D Program of China (Grant No. 2022YFA1204100), the National Natural Science Foundation of China (Grant No. 62488201), the Chinese Academy of Sciences (Grant Nos. XDB33030000 and YSBR-053), and Innovation Program of Quantum Science and Technology (Grant No. 2021ZD0302700).

References

[1] Wieder B J, Bradlyn B, Cano J, Wang Z J, Vergniory M G, Elcoro L, Soluyanov A A, Felser C, Neupert T, Regnault N and Bernevig B A 2022 *Nat. Rev. Mater.* **7** 196
[2] He Q L, Hughes T L, Armitage N P, Tokura Y and Wang K L 2022 *Nat. Mater.* **21** 15
[3] Gilbert M J 2021 *Commun. Phys.* **4** 70
[4] Gong J, Wang H, Ma X P, Zeng X Y, Lin J F, Han K, Wang Y T and Xia T L 2024 *Chin. Phys. B* **33** 077302
[5] Lachman E O, Mogi M, Sarkar J, Uri A, Bagani K, Anahory Y, Myasoedov Y, Huber M E, Tsukazaki A, Kawasaki M, Tokura Y and Zeldov E 2017 *Npj Quantum Mater.* **2** 70
[6] Winnerlein M, Schreyeck S, Grauer S, Rosenberger S, Fijalkowski K M, Gould C, Brunner K and Molenkamp L W 2017 *Phys. Rev. Mater.* **1** 011201
[7] Yu R, Zhang W, Zhang H J, Zhang S C, Dai X and Fang Z 2010 *Science* **329** 61
[8] Chang C Z, Zhang J, Feng X, *et al.* 2013 *Science* **340** 167
[9] Zhao Y F, Zhang R X, Mei R B, Zhou L J, Yi H M, Zhang Y Q, Yu J B, Xiao R, Wang K, Samarth N, Chan M H W, Liu C X and Chang C Z 2020 *Nature* **588** 419
[10] Feng X, Feng Y, Wang J, Ou Y B, Hao Z Q, Liu C, Zhang Z C, Zhang L G, Lin C J, Liao J, Li Y Q, Wang L L, Ji S H, Chen X, Ma X C, Zhang S C, Wang Y Y, He K and Xue Q K 2016 *Adv. Mater.* **28** 6386
[11] Ji Y C, Liu Z, Zhang P, Li L, Qi S F, Chen P, Zhang Y, Yao Q, Liu Z K, Wang K L, Qiao Z H and Kou X F 2022 *ACS Nano* **16** 1134
[12] Zhao Y F, Zhang R X, Sun Z T, Zhou L J, Zhuo D Y, Yan Z J, Yi H M, Wang K, Chan M H W, Liu C X, Law K T and Chang C Z 2024 *Adv. Mater.* **36** 2310249
[13] Ou Y B, Feng Y, Feng X, Hao Z Q, Zhang L G, Liu C, Wang Y Y, He K, Ma X C and Xue Q K 2016 *Chin. Phys. B* **25** 087307
[14] Li W, Claassen M, Chang C Z, Moritz B, Jia T, Zhang C, Rebec S, Lee J J, Hashimoto M, Lu D H, Moore R G, Moodera J S, Devereaux T P and Shen Z X 2016 *Sci. Rep.* **6** 32732
[15] Yao Q, Ji Y C, Chen P, He Q L and Kou X F 2021 *Adv. Phys. X* **6** 1870560
[16] Deng Y, Yu Y, Shi M Z, Guo Z, Xu Z, Wang J, Chen X H and Zhang Y 2020 *Science* **367** 895
[17] Armitage N P, Mele E J and Vishwanath A 2018 *Rev. Mod. Phys.* **90** 015001
[18] Fang C, Weng H, Dai X and Fang Z 2016 *Chin. Phys. B* **25** 117106
[19] Liu E, Sun Y, Kumar N, *et al.* 2018 *Nat. Phys.* **14** 1125
[20] Ye L D, Kang M G, Liu J W, von Cube F, Wicker C R, Suzuki T, Jozwiak C, Bostwick A, Rotenberg E, Bell D C, Fu L, Comin R and Checkelsky J G 2018 *Nature* **555** 638
[21] Feng B J, Zhang R W, Feng Y, Fu B T, Wu S L, Miyamoto K, He S L, Chen L, Wu K H, Shimada K, Okuda T and Yao Y G 2019 *Phys. Rev. Lett.* **123** 116401
[22] Muechler L, Liu E K, Gayles J, Xu Q N, Felser C and Sun Y 2020 *Phys. Rev. B* **101** 115106
[23] Zhang Z, You J Y, Ma X Y, Gu B and Su G 2021 *Phys. Rev. B* **103** 014410
[24] Gao S Y, Xu S, Li H, Yi C J, Nie S M, Rao Z C, Wang H, Hu Q X, Chen X Z, Fan W H, Huang J R, Huang Y B, Pryds N, Shi M, Wang Z J, Shi Y G, Xia T L, Qian T and Ding H 2021 *Phys. Rev. X* **11** 021016
[25] Nie S, Sun Y, Prinz F B, Wang Z, Weng H, Fang Z and Dai X 2020 *Phys. Rev. Lett.* **124** 076403
[26] Süllow S, Prasad I, Bogdanovich S, Aronson M C, Sarrao J L and Fisk Z 2000 *J. Appl. Phys.* **87** 5591
[27] Pan L L, Wang Y H, Ding X, Hu G J, Guo H, Lv S H, Xian G Y, Qi Q, Zhu K, Han Y C, Lei M Y A, Li Z L, Bao L H, Zhang Y, Lin X, Zhu S Y, Peng R, Yang H T and Gao H J 2024 *Appl. Phys. Lett.* **125** 243101
[28] Shen J, Gao J, Yi C, Li M, Zhang S, Yang J, Wang B, Zhou M, Huang R, Wei H, Yang H, Shi Y, Xu X, Gao H J, Shen B, Li G, Wang Z and Liu E 2023 *The Innovation* **4** 100399
[29] Fisk Z, Johnston D C, Cornut B, Molnar S V, Oseroff S and Calvo R 1979 *J. Appl. Phys.* **50** 1911
[30] Snow C S, Cooper S L, Young D P, Fisk Z, Comment A and Ansermet J P 2001 *Phys. Rev. B* **64** 174412
[31] Süllow S, Prasad I, Aronson M C, Sarrao J L, Fisk Z, Hristova D, Lacerda A H, Hundley M F, Vigliante A and Gibbs D 1998 *Phys. Rev. B* **57** 5860
[32] Liu W L, Zhang X, Nie S M, *et al.* 2022 *Phys. Rev. Lett.* **129** 166402
[33] Long G, Xu S, Cai X, Wu Z, Han T, Lin J, Cheng C, Cai Y, Wang X and Wang N 2018 *Nanotechnology* **29** 035204
[34] Liu H, Xue Y, Shi J A, Guzman R A, Zhang P, Zhou Z, He Y, Bian C, Wu L, Ma R, Chen J, Yan J, Yang H, Shen C M, Zhou W, Bao L and Gao H J 2019 *Nano Lett.* **19** 8572
[35] Kumar K, Kumar Y and Awana V P S 2023 *J. Mater. Sci.: Mater. El.* **34** 2302
[36] Lu H Z and Shen S Q 2014 *Proc. SPIE* **9167** 91672E